Cyclic pitch for the control of wind turbine noise amplitude modulation

Franck BERTAGNOLIO[1]; Helge Aa. MADSEN[2]; Andreas FISCHER[3]; Christian BAK[4]

[1,2,3,4] DTU Wind Energy, Technical University of Denmark, Denmark

ABSTRACT

Using experimental data acquired during a wind turbine measurement campaign, it is shown that amplitude modulation of aerodynamic noise can be generated by the rotating blades in conjunction with the atmospheric wind shear. As an attempt to alleviate this phenomenon, a control strategy is designed in form of a cyclic pitch of the blades. As a side effect, it is shown that it is also possible to reduce fatigue load on the blade using this cyclic pitch. The main goal is to reduce both amplitude modulation and fatigue load without compromising the energy harvested from the wind. A simulation tool that can model the different aerodynamic and aeroacoustic aspects of the study is presented. Parameters controlling the cyclic pitch are optimized in order to reduce amplitude modulation and/or fatigue load to a minimum. It is shown that such a minimum can be found and that benefit may be achieved if such a strategy is to be implemented on an actual wind turbine, though at the expense of an increased wear and tear of the pitch control system.

Keywords: Wind turbine, Noise, Amplitude modulation
I-INCE Classification of Subjects Number(s): 14.5.4

1. INTRODUCTION

Over the last decade, the size of wind turbines have considerably increased and modern MW-size wind turbines have rotor diameters approaching 200 m for the largest ones. As a consequence, the aerodynamic noise has become a critical issue when erecting new wind turbines, especially for on-shore projects. Due to local noise regulations, wind turbine or farm installation projects have sometimes to be entirely cancelled. In some other cases, the operating wind turbines have to be derated in order to comply to these regulations resulting in direct loss of revenue for the operators.

Recently, wind turbine noise amplitude modulation has come into focus as an important source of annoyance (1, 2). One of the possible causes for this phenomenon is found to be a combination of the atmospheric wind shear and the rotation of the blades, the latter thus alternatively experiencing low and high wind speeds. This results in a clearly audible modulation of the noise amplitude, sometimes referred to as 'swish' or 'thumping'. In the present article, we will focus only on trailing edge noise as the main source of noise for this phenomenon. However it does not preclude that noise amplitude modulation may be generated by other noise source mechanisms.

In addition to the noise amplitude modulation, wind shear is known to have an effect on blade fatigue loads. Indeed, the alternating low and high inflow speed experienced by the blade results in varying inflow angles onto the blade which are fully correlated along its entire span. Therefore, a periodic aerodynamic loading is applied on the blade at a frequency defined by the rotor rotational speed. In combination with gravity loads and atmospheric turbulence, this mechanism contributes significantly to blade fatigue load and has to be taken into account during wind turbine design. Furthermore, this periodic loading may generate aeroelastic instabilities if not properly dampened.

In this contribution, a simplified control strategy based on a cyclic pitch of the individual blades is proposed in order to mitigate noise amplitude modulation and fatigue loads due to wind shear. The form of this cyclic pitch is optimized using a wind turbine model and an optimization code. Using constraints on the generated power ensures that this control strategy does not result in loss of harvested energy.

The paper is organized as follows. The phenomenon of interest is studied in an experimental context. Then

[1] frba@dtu.dk
[2] hama@dtu.dk
[3] asfi@dtu.dk
[4] chba@dtu.dk

a model that can simulate the relevant aerodynamics and aeroacoustics of the same wind turbine rotor as in the experiment are described. The optimization algorithm used to design the cyclic pitch strategy is introduced. Several optimization configurations are tested and results are presented. The paper ends with some remarks on the present study and possible future work.

2. EXPERIMENTAL EVIDENCE OF ATMOSPHERIC SHEAR EFFECTS ON AERODYNAMICS AND NOISE GENERATION

In this section, measurements performed on a full-scale wind turbine are analyzed. This short study is intended as an illustration of the phenomenon that is addressed in this paper, namely the impact of the atmospheric shear on the aerodynamics of the wind turbine that causes the amplitude modulation phenomenon as the blade experiences alternatively low and high incoming velocities as it rotates.

2.1 The DANAERO experiment

In order to improve the understanding of wind turbine aerodynamic and aeroacoustic phenomena, a measurement campaign on a full-scale MW turbine was conducted in years 2009-2010 as part of the research project entitled DANAERO MW (3, 4). A 40 m wind turbine blade was specifically designed and manufactured by LM Wind Power. It was equipped with a wide array of sensors including structural, aerodynamic and acoustic measurement devices and installed on a 2 MW wind turbine whose main components (i.e. tower, generator, shaft) were also instrumented. In addition, a meteorological mast erected in the vicinity of the wind turbine was used to monitor inflow wind conditions (5).

2.2 Wind turbine aerodynamics

As mentioned earlier, in order to illustrate the amplitude modulation phenomenon that is studied in this article, the chain of events that leads to it are investigated experimentally in this section.

As part of the measurement campaign, the wind velocity was recorded on the meteorology mast at various heights. 10 mins recorded time-series of these velocities at a chosen time during the campaign are averaged and plotted in Fig. 1. The presence of a mean velocity gradient in the atmospheric boundary layer can be clearly observed.

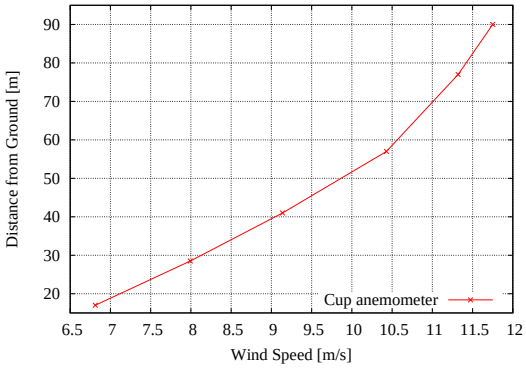

Figure 1 – Atmospheric averaged wind speed profile.

As a consequence of this atmospheric wind shear, two important effects on the wind turbine aerodynamics can be measured. Firstly, the angle of attack is directly related to the inflow velocity. In Fig. 2(a), the time history of the angle of attack measured at two radii on the blade are plotted as a function of the blade azimuth position θ in polar coordinates. Note that the time-series have been averaged over all revolutions of the blade during the same period of time as when the wind speed gradient was observed (see above). In other words, the figure only shows the averaged angle of attack experienced by the blade at each revolution and atmospheric turbulence fluctuations are disregarded. In this figure, $\theta = 0$ when the blade is pointing upward and the blade rotates with increasing θ. It can be seen that the blade experiences lower angles of attack when pointing downward than when pointing upward and that this happens simultaneously at the two blade radii.

Secondly, as the angle of attack increases or decreases in a correlated manner along the blade span, this results in a periodic aerodynamic loading on the blade. This is illustrated by the bending moment in the flapwise direction that is measured at the root of the blade and displayed in Fig. 2(b). As expected, the flapwise bending moment reaches its maximum when the blade is nearly pointing upward (where the angle of attack is maximum, hence the loading on the blade is maximum) and its minimum when the blade is pointing downward.

It should be noted that the periodic fluctuations of the angle of attack and bending moment are not fully symmetric with respect to the vertical axis. Indeed, an azimuth shift of the polar curves can be observed and it is particularly clear for the angle of attack at $r = 31$ m in Fig. 2(a). This can be attributed to a hysteresis effect, the angle of attack response lagging behind (in time and therefore in azimuth location of the blade) the instantaneous variations of the inflow wind speed.

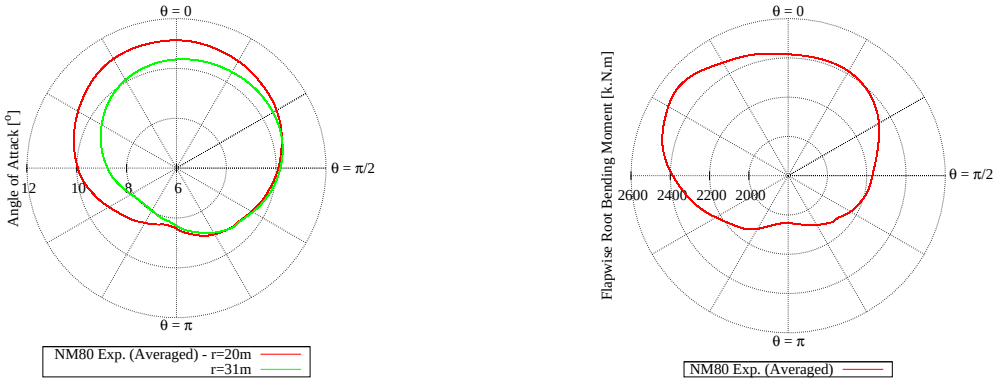

(a) (b)

Figure 2 – Polar plots of: (a) Inflow angle of attack, (b) Bending moments.

2.3 Wind turbine aeroacoustics

Although the aerodynamic noise generated by the wind turbine was not measured, high-frequency microphones were flush-mounted into the instrumented blade at 37 m radius. These were used to measure turbulent surface pressure fluctuations. These microphones have an almost flat frequency response between approximately 100 and 15 kHz. Therefore, they are well-suited to measure spectra that are characteristics of the noise sources in the boundary layer. These surface pressure fluctuations are designated in the litterature as pseudo-noise. Even if their energy content is much larger than the emitted noise, a decrease or increase of their spectral energy at any frequency will have similar effects on the emitted noise in term of spectral energy.

Since we are interested in amplitude modulation of trailing edge noise, a microphone located near the trailing edge of the blade is selected. Time-series of the measured surface pressure fluctuations are recorded over several revolutions of the blade (corresponding to the recording time considered in the previous section). The time-series are truncated into smaller ones which are then binned according to the azimuth position of the blade at the specific recording time of these smaller time-series. Finally, all smaller time-series are Fourier transformed and spectra belonging to the same bin are averaged together. In our case, four bins were created by dividing the rotor plane into four sections of identical 90° azimuth intervals. The first one is centered on the blade pointing upward at $\theta = 0$. The second is centered on the blade descending and parallel to the ground at $\theta = \pi/2$. The third and fourth ones are centered on the blade pointing downward and the blade ascending and parallel to the ground, respectively ($\theta = \pi$ and $3\pi/2$).

The measured and averaged surface pressure spectra for the four bins are displayed in Fig. 3. Two extreme cases depending on whether the blade is pointing upward or downward can be observed. In the first case, spectral energy is higher in the low frequency range and lower in the high frequency range, and vice versa in the second case. For the blade ascending or descending, the results are somehow in between the two extreme cases. However, there are some differences which can be explained by the same hysteresis effect that was observed in the previous section. Indeed, the boundary layer turbulence does not instantaneously respond to the changes in inflow conditions as the blade rotates and experiences varying wind speed, in the same way as for the angle of attack.

From measurements performed in wind tunnel (6), it can easily be verified that the observed surface pressure spectral energy redistributions between low and high frequencies can be directly related to the variations of the angle of attack. These spectral energy redistributions will furthermore certainly be reflected on the far-field noise in a similar manner. The above described mechanism is readily the amplitude modulation phenomenon that we are interested in.

3. ROTOR MODEL

In this section, the models used to simulate the rotor aerodynamics and noise generation are described.

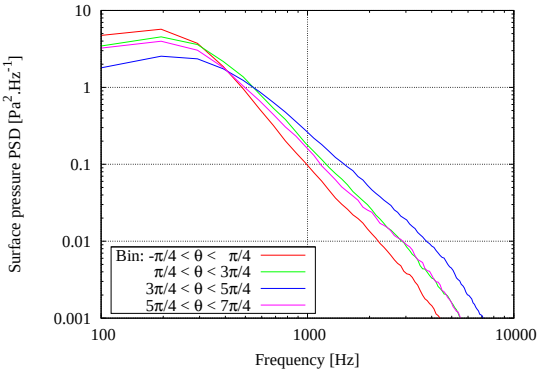

Figure 3 – Surface pressure spectra binned according to blade azimuth position.

3.1 Rotor blade momentum model

The present model for the rotor aerodynamic is based on the classical Blade Element Momentum (BEM) theory (7). The fluid volume flowing across the rotor is discretized into co-axial flow tubes on which this one-dimensional theory is applied. The local aerodynamic loading (lift and drag) on a blade airfoil section at a particular radius and azimuth location of the rotor plane is known as a function of the local inflow conditions, which are primarily defined by the incoming wind velocity at this particular height and the angular velocity of this section due to rotation at this particular radius. The solution method consists in finding an equilibrium between the local loading on the blade section and the local induction factors (along the mean flow direction and along the angular velocity vector) that are used to account for the local deformation of the flow created by the blade loading. This local deformation in turn modifies the local relative inflow velocity and angle of attack on the blade airfoil section and thereby the aerodynamic loading. Equilibrium is reached through an iterative procedure. Corrections for tip and and root losses using Prandtl's corrective function (8) are included in the present model.

The geometric and operational characteristics of the wind turbine, including yaw, tilt, blade pitch, blade twist/thickness/chord radial distributions, and rotational speed can be specified and are taken into account accordingly at the local rotor locations. As for the incoming flow conditions, mean wind speed, wind shear, inflow turbulence intensity and integral length scale can be similarly specified to determine the local flow conditions across the rotor plane.

As a closure for this BEM rotor model, the aerodynamic loading on the blade airfoil sections as a function of the local angle of attack has to be specified. In order to evaluate rotor loads and performances such as thrust, torque, power, etc., engineers usually resort to tabulated 2D data for the particular airfoil profiles used along the span of the blade. These data may for example originate from wind tunnel measurements and are usually corrected for 3D effects that generally become significant near the root of the blade. In our case, an additional approach is also used. Since the trailing edge noise model introduced later in Section 3.2 requires informations about the turbulent boundary layer characteristics (such as boundary layer velocity profile and thickness near the trailing edge), the flow is assumed to be locally two-dimensional and the XFOIL code (9) is used at each blade section to evaluate iteratively the local aerodynamic loading and induction as described above. Note that if the former approach using tabulated 2D data for calculating the rotor aerodynamics is used, then the local trailing edge boundary layer characteristics are also obtained using XFOIL results, but for which the local inflow velocity and angle of attack are directly extracted from the rotor calculation with tabulated data.

For all calculations, the rotor plane is discretized into 16 blade sections along the blade span from the root to the tip and 16 angular sections in azimuth.

3.2 Noise model

The hypothesis behind this study is based on the fact that amplitude modulation is generated by the combination of trailing edge noise as the main source of noise and the rotation of the blade as the mechanism for modulation of the noise amplitude. Therefore, only trailing edge noise will be simulated in the results presented in this article.

Trailing edge noise is produced by the convection above the trailing edge of the vortices generated in the turbulent boundary layer developing on an airfoil surface, resulting in a scattering phenomenon. In our case, the so-called TNO model originally derived by Parchen (10) is used. It is mainly based on previous works as follows. Using the total enthalpy as a main unknown for formulating an equivalent to the Lighthill

analogy (11), Howe (12) proposed a theory that describes the trailing edge noise mechanism. Combining the previous theory with the derivation of the surface pressure spectrum beneath a turbulent boundary layer as originally proposed by Kraichnan (13) and extended by Blake (14), Parchen (10) (see also Moriarty *et al* (15)) develops a methodology, the so-called TNO model, to predict trailing edge noise based on 2D Reynolds-Averaged Navier-Stokes calculations of airfoil flows.

Recently, the authors derived an improved version of the model that accounts for the turbulence anisotropy in the boundary layer in the presence of an adverse pressure gradient (16, 6). This version of the model will be used in this article. In addition, since the present study will involved an optimization technique that will require numerous model evaluations, the Computational Fluid Dynamics approach of the original TNO model will be replaced by a faster and simpler approach for boundary layer calculation during this optimization process. The XFOIL software will be used for that purpose (9). It is based on a panel method to compute the flow around the airfoil and it is coupled to an integral boundary layer formulation. Detail about its coupling to the TNO noise model has been described in earlier works (15, 17).

The emission noise is calculated at each radial section and each azimuth angle location of the discretized rotor plane as defined in the previous section. The local aerodynamic characteristics calculated by the BEM method and the XFOIL code on this mesh are used as input for the trailing edge noise model. Note that the far-field noise that will be used to define the cost function during the optimization procedure in Section 5 is estimated at 50 m downstream of the rotor at hub height. This is done in order to minimize the influence of directivity effects on the results. Indeed, these effects are known to produce a localization of the aerodynamic blade noise at specific locations on the rotor disk (18). As the blades rotate, this leads to an acoustic behaviour associated to amplitude modulation. However, in the present work we are not interested in this particular phenomenon which is more dependent on the receiver's location than the pitch control strategy.

4. OPTIMIZATION METHODOLOGY

The optimization problem that will be defined later in this paper will require the minimization of a cost function subject to constraints. However, no information will be available concerning the cost function and constraints derivatives with respect to the design variables. An algorithm able to deal with this kind of problem is presented below.

4.1 Generalized pattern search method

The optimization algorithm used in this work is an in-house implementation of the method proposed by Booker *et al* (19). It is an extension of the pattern search method which convergence has been proven by Audet *et al* (20).

The basic idea behind the pattern search framework is that the design space is restricted to lie on a mesh which can be refined as a local minimum is approached. Therefore, cost function and constraints are only evaluated for points located on this mesh (or meshes if refinement is considered). The algorithm involves two steps: a 'search' step and a 'poll' step. Each step is deemed successful if it finds a mesh point that improves the cost function and satisfies the constraints. The exploratory search step may use virtually any strategy to attempt to reduce the cost function. The goal of this step is to increase the convergence rate of the method toward a global or local minimum, but is not necessary for the convergence of the algorithm itself. Convergence is ensured by the poll step where points neighbouring the current best point on the mesh are evaluated to check if the current best point is a mesh local optimum. The set of neighbouring poll points are required to generate a $n+1$ positive basis (where n is the dimension of the design space) in order to ensure convergence (20).

The iterative procedure consists in performing search steps until one fails, i.e. until no mesh point improving the cost function is found. Then, a poll step is performed. If it is successful, then the algorithm switches back to search steps as above. Note that the mesh may be coarsened at this stage. If no neighbouring point improving the cost function is found during a poll step, then the mesh is refined and the above search/poll steps sequence is continued on this finer mesh. This process is iterated until the mesh refinement has reached a user-defined limit and the poll step is unsuccessful. The issue of handling the constraints and proving convergence has been discussed by Audet *et al* (21).

Note that in our case, various strategies for the search step are implemented. In particular using the classical Simplex method to generate exploratory directions were found to be quite effective for the present kind of problems. But a detailed description of these strategies is beyond the scope of this paper.

5. OPTIMIZED PITCH CONTROL

The design procedure used in this paper makes use of the optimization algorithm introduced in the previous section and is based on the wind turbine aerodynamic and noise model presented in Section 3. A model configuration with similar conditions as the test wind turbine which was discussed in Section 2.1 is used as reference.

5.1 Choice of design variables

The control strategy proposed within this article is defined as an individual cyclic pitch of the blades around a given fixed pitch. In other words, the same pitch variation as a function of azimuth is applied to each blade during a revolution according to their respective azimuth locations. Furthermore, the pitch function as a function of the azimuth position is assumed sinusoidal with a period equal to one revolution of the blade. Therefore, the design variables for the optimization algorithm are the amplitude of the pitch variation and its phase relative to a reference position of the blades (say, the blade pointing upward).

Yaw is known to have an effect on cyclic loads. Therefore, a yaw error was introduced as a design variable in the optimization algorithm, in addition to the two previous ones, in order to measure its impact on the results. Although a small yaw error (of the order of 2 to 3°) can be beneficial, differences in the performances of the resulting optima were found to be only marginal and are not presented here.

5.2 Cost function and constraints

As mentioned earlier, the main goal of this study is two alleviate two phenomena undesirable for wind turbine operation:

- aerodynamic noise amplitude modulation, and
- cyclic loading on the blades.

To achieve this, this two aspects are quantified and the cost function for the optimization algorithm is defined from these values.

The wind turbine model gives access to the trailing edge noise spectra generated by each blade section as a function of the azimuth position of the blade on the discretized rotor disk (see Section 3). These noise spectra can firstly be integrated across the whole frequency range yielding a sound pressure level (SPL). Secondly, the SPLs can be further integrated along the blade span to form an equivalent SPL characteristics of the whole blade and function of its azimuth location. Noise amplitude modulation is then quantified as the difference between the maximum and the minimum of the blade SPL during one revolution of the blade.

Note that using the maximum of the sound pressure spectral energy (instead of integrating across frequency) was also tested. However this yielded very similar results. Indeed, most of the spectral energy is located near the frequency where it reaches its maximum.

Similarly, the aerodynamic loading on each blade sections can be integrated over the blade span to define the moment exerted at the root of the blade. Then, the periodic amplitude of the resulting azimuth dependent time-series is used as a measure of the cyclic loading.

Both quantities are normalized by the equivalent quantity for the reference turbine, which will be used as an initial guess for the iterative optimization algorithm. Three cost functions are defined. The first one consists only of the cost associated to the noise modulation. The second one consists only of the cost associated to the aerodynamic loading. And the third one is created by equally weighting the two normalized values.

Finally, constraints are enforced to preserve the characteristics of the reference turbine model. The first one consists in ensuring that the power generated by the wind turbine with cyclic pitch cannot be smaller than the one generated by the reference turbine model. Two additional constraints ensure that the maximum flapwise bending moment and the maximum SPL at all blade azimuth locations are smaller than those calculated for the reference turbine.

5.3 Results

The results from the optimization procedure are displayed in Figs. 4(a-b). The first figure shows the integrated SPL as a function of the azimuth for the three types of cost function as defined above, whereas the second shows the flapwise bending moment. It can be seen that the three cost function definitions achieve amplitude reductions for the two quantities of interest. As expected, equally weighting the cost function gives intermediary results.

Quantitative results are given in Table 1 where the rotor power together with the amplitude ranges of the SPL and the flapwise bending moment are reported. It can be seen that significant reductions of noise amplitude modulations are achieved in the two cases where the cost function includes the SPL. Note that these two optima also yield a small increase in rotor power. Surprisingly, the case for which the cost function only involves the flapwise bending moment results in lower reduction of the moment amplitude than the previous cases. This is attributed to the fact that the iterative optimization algorithm probably got stucked at

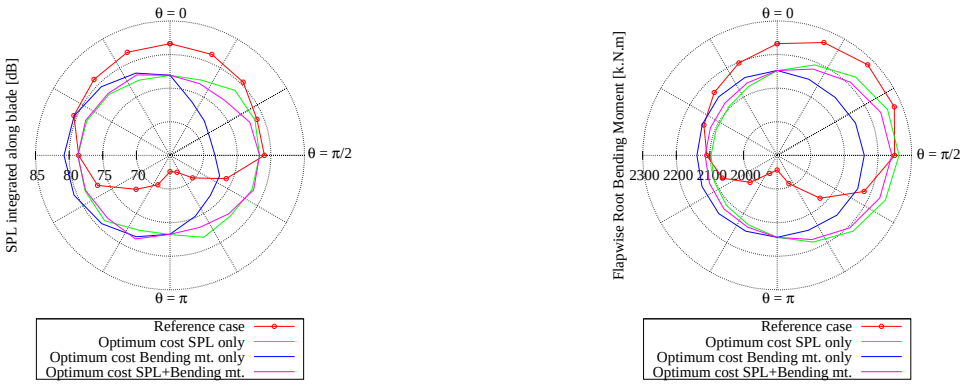

(a) (b)

Figure 4 – Polar plots of: (a) SPL integrated along blade; (b) Flapwise bending moment.

a local optimum and failed to achieve further reduction of the cost function.

Table 1 – Performances for reference case and optimized cyclic pitch operational conditions.

Case	Power, kW	SPL amplitude, dB	Flapwise mt. amplitude, kN m
Reference	1540	14.20	337.5
Cost SPL only	1554	1.965	165.8
Cost bending mt. only	1540	9.305	207.1
Cost SPL+bending mt.	1553	2.177	126.7

6. FINAL REMARKS

Using a wind turbine simulation tool, it was shown in this paper that individual cyclic pitch of the blades of an horizontal axis wind turbine can be used to reduce both noise amplitude modulation and blade fatigue load without reducing the energy output of the turbine. The specific control strategy for the cyclic pitch was optimized ultimately yielding potential improvement of the cost of energy of a wind turbine.

Nevertheless, the results obtained in the present study remain theoretical and have to be implemented on an actual wind turbine to validate the potential of such a control strategy. Indeed, a cyclic pitch has a significant impact on the design and choices made for the mechanical devices that actuate the pitch of the blade, which costs have to be evaluated to complete this study.

Finally, it is important to point out the fact that the present optimization study was performed in ideal conditions since atmospheric turbulence was not included in the simulation. In the case of a large atmospheric turbulence intensity, its impact on the flapwise bending moment and on the noise amplitude modulation may exceed that of the wind shear combined with the rotation of the blade as described in this paper. This may render the above control strategy useless for the specific purpose for which it was implemented. Such analysis will be performed in future work.

ACKNOWLEDGEMENTS

Authors would like to acknowledge the support of the Danish Energy Agency (Energistyrelen) that funded the DANAERO MW and DANAERO MW II projects (Contract nos. ENS-33033-0074 and ENS-64009-0258).

REFERENCES

1. Bowdler D. Amplitude Modulation of Wind Turbine Noise, A Review of the Evidence. Institute of Acoustics Bulletin (UK). 2008;33(4).

2. Oerlemans S, Smith MG, White P, von Hünerbein S, King A, Piper B, et al. Wind Turbine Amplitude Modulation: Research to Improve Understanding as to its Cause and Effect. RenewableUK, United King-

dom; 2013. Available online: http://www.renewableuk.com/en/publications/reports.cfm/wind-turbine-amplitude-modulation.

3. Bak C, , Madsen HA, Paulsen US, Gaunaa M, Sørensen NN, et al. DAN-AERO MW: Detailed Aerodynamic Measurements on a Full Scale MW Wind Turbine. In: Proc. EWEA 2010. Warzaw, Poland; 2010. .

4. Madsen HA, Bak C, Paulsen US, Gaunaa M, Fuglsang P, Romblad J, et al. The DAN-AERO MW Experiments. In: Proc. of the 48^{th} AIAA Aerospace Sciences Meeting Including The New Horizons Forum and Aerospace Exposition. . Orlando (FL); 2010. .

5. Bak C, Madsen HA, Gaunaa M, Skrzypinski W, Paulsen U, Møller R, et al. DANAERO MW: Instrumentation of the NM80 2.3MW wind turbine including the LM 38.8 m blade and the meteorology mast at Tjæreborg. Risø-DTU, Roskilde, Denmark; 2010.

6. Bertagnolio F, Fischer A, Zhu WJ. Tuning of Turbulent Boundary Layer Anisotropy for Improved Surface Pressure and Trailing-Edge Noise Modeling. Journal of Sound and Vibration. 2014;333(3):991–1010.

7. Glauert H. Airplane Propellers. vol. Aerodynamic Theory Volume IV. W. F. Durand, The Dover Edition (UK); 1963.

8. Leishman JG. Principles of Helicopter Aerodynamics. vol. Chapter 2. Cambridge University Press (UK); 2000.

9. Drela M. XFOIL: An Analysis and Design System for Low Reynolds Number Airfoils. In: Low Reynolds Number Aerodynamics. vol. 54. Mueller, T.J. (ed.), Lecture Notes in Engineering, Springer-Verlag, Berlin; 1989. p. 1–12.

10. Parchen R. Progress report DRAW: A Prediction Scheme for Trailing-Edge Noise Based on Detailed Boundary-Layer Characteristics. TNO Institute of Applied Physics, The Netherlands; 1998.

11. Lighthill MJ. On Sound Generated Aerodynamically. I. General Theory. Proceedings of the Royal Society London A. 1952;211(1107):564–587.

12. Howe MS. A Review of the Theory of Trailing Edge Noise. J Sound Vib. 1978;61(3):437–465.

13. Kraichnan RH. Pressure Fluctuations in Turbulent Flow over a Flat Plate. J Acoust Soc Am. 1956;28(3):378–390.

14. Blake WK. Mechanics of Flow-Induced Sound and Vibration, Vol.I and II. vol. in Applied Mathematics and Mechanics. Frenkiel, F.N. and Temple, G. (eds.), Academic Press; 1986.

15. Moriarty P, Guidati G, Migliore P. Prediction of Turbulent Inflow and Trailing-Edge Noise for Wind Turbines. In: Proc. of the 11^{th} AIAA/CEAS Aeroacoustics Conf. AIAA Paper 2005-2881. Monterey, CA; 2005. .

16. Bertagnolio F. Experimental Investigation and Calibration of Surface Pressure Modeling for Trailing Edge Noise. In: Proc. of Inter-Noise 2011 Conf. Osaka, Japan; 2011. .

17. Bertagnolio F, Madsen HA, Bak C. Trailing Edge Noise Model Validation and Application to Airfoil Optimization. J Sol Energy Eng. 2010;132(3):031010(9 pages).

18. Oerlemans S, Sijtsma P, López BM. Location and Quantification of Noise on a Wind Turbine. J Sound Vib. 2007;299(5-6):869–883.

19. Booker AJ, Dennis JJE, Frank PD, Serafini DB, Torczon V, Trosset MW. A Rigorous Framework for Optimization of Expensive Functions by Surrogates. Structural Optimization. 1999;17:1–13.

20. Audet C, Dennis JJE. Analysis of Generalized Pattern Searches. SIAM Journal on Optimization. 2003;13:889–903.

21. Audet C, Dennis JJE. A Pattern Search Filter Method for Nonlinear Programming Without Derivatives. SIAM Journal on Optimization. 2004;14(4):980–1010.